ARTICLE   OPEN

Many-body effects in doped WS$_2$ monolayer quantum disks at room temperature

T. N. Lin[1,4], S. R. M. Santiago[1,4], S. P. Caigas[1], C. T. Yuan[1], T. Y. Lin[2], J. L. Shen[1]* and Y. F. Chen[3]

Due to strong Coulomb interactions, reduced screening effects, and quantum confinement, transition-metal dichalcogenide (TMD) monolayer quantum disks (MQDs) are expected to exhibit large exciton binding energy, which is beneficial for the investigation of many-body physics at room temperature. Here, we report the first observations of room-temperature many-body effects in tungsten disulfide (WS$_2$) MQDs by both optical measurements and theoretical studies. The band-gap renormalization in WS$_2$ MQDs was about 250 ± 15 meV as the carrier density was increased from $0.6(\pm 0.2) \times 10^{12}$ to $8.3(\pm 0.2) \times 10^{12}$ cm^{-2}. We observed a striking exciton binding energy as large as 990 ± 30 meV at the lowest carrier density, which is larger than that in WS$_2$ monolayers. The huge exciton binding energy in WS$_2$ MQDs is attributed to the extra quantum confinement in the lateral dimension. The band-gap renormalization and exciton binding energies are explained using efficient reduced screening. On the basis of the Debye screening formula, the Mott density in WS$_2$ MQDs was estimated to be $\sim 3.95 \times 10^{13}$ cm^{-2}. Understanding and manipulation of the many-body effects in two-dimensional materials may open up new possibilities for developing exciton-based optoelectronic devices.

npj 2D Materials and Applications (2019)3:46 ; https://doi.org/10.1038/s41699-019-0129-z

INTRODUCTION

Due to the reduced dielectric screening and relatively heavy particle band masses, few-layered transition-metal dichalcogenide (TMDs) form tightly bound electron–hole pairs (excitons) with binding energies up to hundreds of meV, which is much larger than that in conventional bulk semiconductors.[1–3] The strongly bound excitons produce a variety of interesting multiparticle excitations such as charged excitons (trions), biexcitons, and exciton–trion complexes.[3–5] Because of efficient Coulomb interactions, few-layered TMDs are strongly interacting systems even in high carrier densities, thus, they provide an ideal vehicle to study fundamental many-body physics, such as band-gap renormalization and the Mott transition.[2,6–8]

Carrier doping allows us to modulate the band structure of TMDs and manipulate their properties. By increasing the doping in few-layered TMDs, carriers can occupy the phase space of the conduction (valence) band at the K/K' points leading to the Pauli blocking effect, as originated from the Pauli exclusive principle. In addition, the band-gap and exciton binding energy were renormalized due to the exchange interaction and efficient screening in the dense carriers.[7–9] At very high carrier densities of $\sim 10^{13}$ cm^{-2}, the excitons in TMDs are expected to be ionized completely due to efficient many-particle interactions and the formation of free electron–hole plasma, known as the Mott transition.[6,10] Recently, the above effects have attracted great attention in few-layered TMDs; for example, the change of exciton binding energies in the monolayer tungsten disulfide (WS$_2$) of more than 100 meV has been demonstrated.[6] A band-gap renormalization of over 150 meV and an exciton binding energy as large as 790 meV have also been demonstrated in monolayer molybdenum disulfide (MoS$_2$) through photoluminescence excitation (PLE).[2] With intense optical pulses, a Mott transition from excitons to free carriers has been observed accompanied by a huge band-gap renormalization.[7] To date, most of the experiments involving the many-body effects in TMDs have been performed at cryogenic temperature (50–80 K).[2,6] It is desirable to understand many-body physics in TMDs at room temperature, in order to implement two-dimensional materials for developing exciton-based optoelectronic devices, such as excitonic light emitting devices and exciton lasers.[5,7]

To date, the studies of many-body effects on TMD materials have been concentrated on monolayers or bilayers, while little attention has been given to TMD monolayer quantum disks (MQDs), which are monolayered TMDs with lateral dimensions in nanoscale. Compared to few-layered TMDs, large direct transition energies and spin–valley coupling can be intuitively anticipated in TMD MQDs.[11] Exciton binding energy in TMD MQDs is expected to exceed that in few-layered TMDs because of the quantum confinement in the lateral dimension. A large exciton binding energy means the high thermal stability of excitons, which makes them become promising candidates for observing room-temperature many-body effects. This work observed the renormalization of the quasi band-gap and reduction of the exciton binding energy in WS$_2$ MQDs using room-temperature PLE and the absorption spectra. On the basis of carrier screening, we discuss the mechanism that causes the carrier-induced band-gap renormalization and the reduced exciton binding energies.

RESULTS

TEM and AFM measurements

The transmission electron microscopy (TEM) images of the synthesized WS$_2$ MQDs with carrier density (p) of $0.6(\pm 0.2) \times 10^{12}$ cm^{-2}, $3.0(\pm 0.2) \times 10^{12}$ cm^{-2}, and $8.3(\pm 0.2) \times 10^{12}$ cm^{-2} are shown in Supplementary Fig. S1, which exhibit monodispersed distribution with an average size of $\sim 5.0 \pm 1.0$ nm. Statistical analyses of the TEM images demonstrate Gaussian distribution curves as shown in Supplementary Fig. S2. Atomic force

---

[1]Department of Physics and Center for Nanotechnology, Chung Yuan Christian University, Chung-Li, Taiwan. [2]Institute of Optoelectronic Sciences, National Taiwan Ocean University, Keelung, Taiwan. [3]Department of Physics, National Taiwan University, Taipei, Taiwan. [4]These authors contributed equally: T. N. Lin, S. R. M. Santiago.
*email: jlshen@cycu.edu.tw

microscopy (AFM) of the WS_2 MQDs was performed to characterize the height profile of the synthesized WS_2 MQDs and the result is displayed in Supplementary Fig. S3. The average heights of MQDs were found to be between 0.7–1.0 nm, which correspond to monolayer WS_2.

PL, PLE and Absorbance measurements

The blue line in Fig. 1 shows the photoluminescence (PL) spectrum of the WS_2 MQDs with p of $0.6(\pm0.2) \times 10^{12}$ cm^{-2} under the excitation wavelength of 260 nm. A PL emission with double-peak features located at around 2.69 and 2.85 eV was observed. The double-peak PL likely arise from the recombination due to excitons bound to different defect and/or surface states (DX states).[2,12–14] Similar multiple defect peaks have been observed in other TMD materials.[13,14] The full width at half maximum (FWHM) of the PL in WS_2 MQDs is rather broad (about 700 meV), and this feature was attributed to a combination of cascade PL signals due to multiple DX states. Supplementary Fig. S4 shows the PL spectra of WS_2 MQDs with $p = 0.6(\pm0.2) \times 10^{12}$ to $8.3(\pm0.2)10^{12}$ cm^{-2} under the excitation wavelength of 260 nm. When p was increased, all the PL spectra displayed similar peak energies; however, the PL intensities varied significantly; it increased from $p = 0.6(\pm0.2)10^{12}$ to $1.1(\pm0.2) \times 10^{12}$ cm^{-2}, but decreased after p exceeded $1.1(\pm0.2) \times 10^{12}$ cm^{-2}. The PL intensity enhancement is attributed to the increase of carrier densities due to the diethylenetriamine (DETA) doping. The PL reduction could be explained by the generation of defects during the doping processes, which produced nonradiative centers and weaken the PL intensity. Another possible explanation of the PL reduction is the nonradiative recombination via the Auger effect, as the Auger processes are very efficient in TMDs.[15]

The red line in Fig. 1 shows the PLE spectrum of the WS_2 MQDs ($p = 0.6(\pm0.2) \times 10^{12}$ cm^{-2}) under detection with emission energy of 2.75 eV. A clear PLE peak of energy around 3.12 ± 0.02 eV and a FWHM of ~200(±10) meV were observed. To determine the origin of the PLE peak, the absorption spectrum of the WS_2 MQDs was

also measured and displayed as the green line in Fig. 1. Two peaks at around 3.21 ± 0.02 and 3.73 ± 0.02 eV were observed in the absorption spectrum, and their energies are in agreement with those of the previously reported WS_2 MQDs (3.15 and 3.72 eV).[11] On the basis of the assignment in ref. [11], the absorption peaks at 3.21 ± 0.02 and 3.73 ± 0.02 eV are attributed to the A- and B-excitons, respectively, whose energy separation is due to the spin-orbit splitting of the top of the valence band at the K point. Accordingly, we assign the 3.12 ± 0.02 eV peak in PLE to be the A-exciton. It is noted that, while both the A- and B-excitons were observed in the absorption spectrum, only the A exciton was observable in PLE. In general, PLE is a luminescence technique to investigate the absorption properties of a material through relaxation processes, thus, PLE provides the information of both the absorption properties and the relaxation processes. During the relaxation processes in our case, the photogenerated B-excitons preferably coupled with A-excitons, and transformed to A-excitons because the absorbing states lie in the same region of the Brillouin zone.[2] Thus, as most of the B-excitons are transformed to A-excitons and emit PL with higher energies, the detection of the PLE signal at the DX state was greatly reduced. A similar absence of B-excitons for the defect PL yield in monolayer MoS_2 has been previously reported.[2] In addition to the A-exciton, a small peak at ~3.90 eV was observed in the PLE spectrum, which first increased, but decreased after p exceeded $1.0(\pm0.2) \times 10^{12}$ cm^{-2}. This peak could be attributed to the C-exciton transition.[15] The enhancement of the C-exciton with increased carrier densities is attributed to the DETA doping, while the decreased PL of C-excitons could be attributed to the generation of defects during the doping processes or the Auger effect, as p was considerably increased.

It is noteworthy that, the energy of the PL peak does not correspond to that of the A-exciton in the absorption spectra, which is different from previous studies in monolayer TMDs.[16,17] The large deviation between the PL and absorption spectra is likely a signature of the MQD formation. During the synthesis processes, WS_2 nanoflakes are cut into small pieces and produce many defects such as dangle bonds or vacancies at/or near the surface of MQDs. These surface defects lead to surface states or edge states and are expected to contribute to PL with the energies lower than exciton energies. Thus, the energy of the PL peak is lower than that of excitons in the absorption spectra. Similar features have been observed in MoS_2 nanoclusters.[12]

Figure 2a displays the PLE spectra of the WS_2 MQDs with varying p ($0.6(\pm0.2) \times 10^{12}$ to $8.3(\pm0.2) \times 10^{12}$ cm^{-2}) under detection with the emission energy of 2.75 eV. The PLE spectra of the WS_2 MQDs under detection energies of 2.95, 2.85, and 2.67 eV were also measured, as shown in Supplementary Fig. S5. The PLE spectra under the detection energies of 2.95 and 2.85 eV are similar to those of 2.75 eV. Regarding the detection energy of 2.67 eV, the A-exciton signal interferes with the peak from DX states, and produced a merged and broadened PLE, which is difficult to discriminate from the exciton peak. Thus, this study
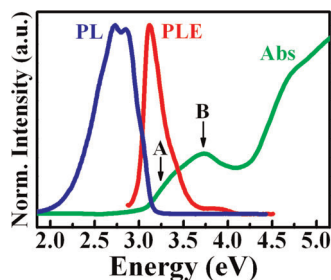

Fig. 1 PL, PLE, and absorbance characterization. Room-temperature PL, PLE, and absorption spectra of WS_2 MQDs with the carrier density of 0.63×10^{12} cm^{-2}.
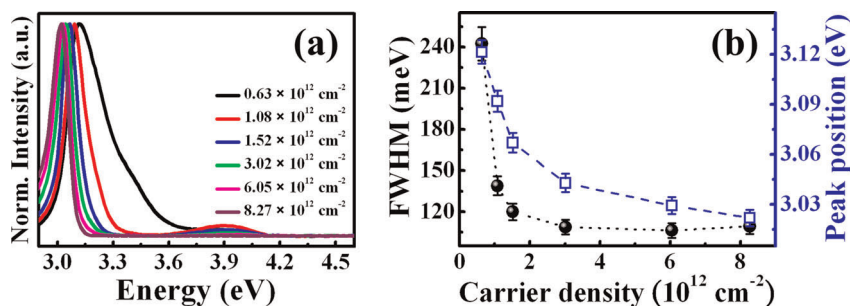

Fig. 2 PLE characterization and analysis. **a** Room-temperature PLE spectra of the WS_2 MQDs with different carrier densities under the detection with luminescence energy of 2.75 eV. **b** E_{exc} and FWHM of the A-exciton as a function of carrier densities in WS_2 MQDs. The dashed and dotted lines are a guide for the eye.

investigated the PLE of WS$_2$ MQDs under detection with the emission energy of 2.75 eV. To further confirm the PL spectra, the PL and PLE measurements of the MoS$_2$ MQDs with varying DETA doping are also carried out under the excitation wavelength of 260 nm, as displayed in Supplementary Fig. S6. All the above results reveal a redshift of the PLE peak (A-exciton) as p is increased. The redshift of the exciton energy (E_{exc}) in A-excitons with increasing p is shown in the open squares of Fig. 2b. One possible interpretation for the redshift in the PLE peak with different p is the energy shift of quantum confinement, which is due to the non-uniform diameter distribution in MQDs. However, according to our TEM results (Supplementary Fig. S2), the size distribution of WS$_2$ MQDs is comparable with that of WS$_2$ MQDs with different p; therefore, the energy shift of PLE due to the size-dependent effect should be ruled out. In general, the increase of carrier densities in semiconductors may induce four effects on the E_{exc}.[6,8,18] First, band-gap renormalization, which is due to the many-body exchange and correlation interaction induced shrinkage of the quasiparticle band-gap (E_g).[18] Second, the Pauli blocking causes a reduction of the exciton binding energy due to the fermionic nature of carriers and the carrier occupation.[6] Third, the carrier screening of the Coulomb interaction reduces the strength of Coulomb force, leading to a decrease of the exciton binding energy.[8] Finally, coupling between the intervalley (shortwave) plasmons and the exciton in the TMD monolayers may yield a shift of the exciton peak.[19–21] However, the effect of intervalley plasmons was found to be more pronounced in electron-doped TMDs,[19–21] not in hole-doped materials as in our work presented here. The contribution of E_{exc} is determined by the interplay between band-gap renormalization and the latter three effects (the Pauli blocking, screening, and intervalley plasmons), which induce a redshift and a blueshift, respectively. Incomplete compensation of these effects may produce a net peak shift of E_{exc}. Recent experimental and theoretical studies indicate that the dependence of exciton energies on the carrier density in TMD monolayers can result in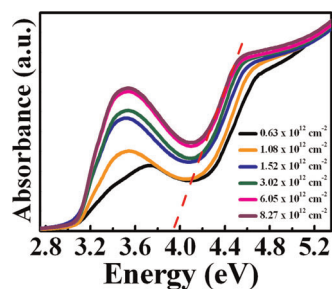 a redshift, blueshift, or combination of both.[2,6,8,19,22–25] In our case, the redshift of E_{exc} in Fig. 2b reveals that the band-gap renormalization dominates the other mechanisms in WS$_2$ MQDs as p was increased. Regarding our WS$_2$ MQDs, the nanoscale size in the lateral dimension can contribute extra quantum confinement effect, which leads to more pronounced effect for band-gap renormalization than that in the TMD monolayers. It is noted that, the 3.90 eV peak (C-transition) in PLE first increased, but decreased after p was increased. Similar to the result in the defect PL (Supplementary Fig. S4), the enhancement and reduction of PLE could be due to the doping and Auger effects, respectively.

The FWHM of the A-exciton peak in the PLE of WS$_2$ MQDs was found to decrease as p was increased, as displayed in the circles of Fig. 2b. Recently, a broadband spectra above the exciton peak of the PLE or reflectance in TMDs related to the Rydberg progression of excitons have been reported.[26,27] The broadband of excitation energies was attributed to the efficient interexcitonic coupling from higher-energy states to the ground state.[26] We suggest that the anomalous narrowing of FWHM with increasing p could accounted for the doping-induced screening effect on the higher exciton excited states. In light of the calculation using the first-principle Bethe–Salpeter equation, the higher exciton excited states at high doping densities have a weaker bound state, as compared to the exciton 1s state.[9] The weaker bound state feels a stronger effective screening and becomes unstable. As the doping density kept increasing, the higher exciton excited states disappeared quickly and left the 1s state as the only exciton state.[9] Thus, the FWHM of PLE in WS$_2$ MQDs was observed to decrease with the increasing p, as shown in Fig. 2b.

Figure 3 shows the absorption spectra of the WS$_2$ MQDs with varying p (0.6($\pm$0.2) $\times$ 10^{12} to 8.3($\pm$0.2) $\times$ 10^{12} cm^{-2}). A broad absorption peak between 3.0 and 4.0 eV, and a step-like absorption band after 4.0 eV, were observed. The former broad peak in the absorption spectrum is related to the combination of A- and B-excitons. On the other hand, as the step-like absorption is a signature of noninteracting electrons in two dimensions, the step-like absorption feature after ~4.0 eV allows us to extract the spectral positon of continuum unbound states.[9] Thus, by extrapolating the linear portion of the step-like absorption threshold, we can estimate the onset of continuum absorption of free-carrier excitation (E_{con}). The closed circles in Fig. 4a show the obtained E_{con} of the WS$_2$ MQDs as a function of p, where the E_{con} decreased rapidly as p increased from 0.6($\pm$0.2) $\times$ 10^{12} to 1.5 ($\pm$0.2) $\times$ 10^{12} cm^{-2}, and then, decreased gradually with p higher than 1.5($\pm$0.2) $\times$ 10^{12} cm^{-2}.

Band-gap renormalization

Regarding the WS$_2$ MQDs with dense carriers, E_{con} is larger than E_g due to Pauli blocking, as caused by an upward shift by carrier densities (Fermi level) with increasing p, and shown in Fig. 4b. By assuming the 2D parabolic dispersion around the K point, the Fermi wave vector can be represented by $k_F = (4\pi n/g_s g_v)^{1/2} = (4\pi p/g_s g_v q)^{1/2}$,

Fig. 3 Absorbance characterization and analysis. Room-temperature absorption spectra of the WS$_2$ MQDs with different carrier densities. The intersection of the dashed line and the x-axis represents the onset of E_{con}.
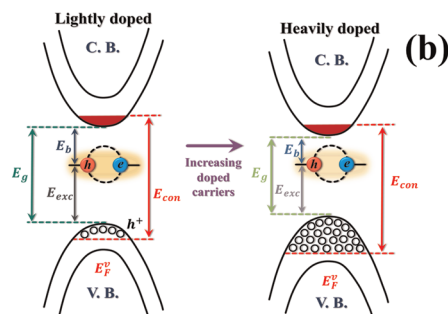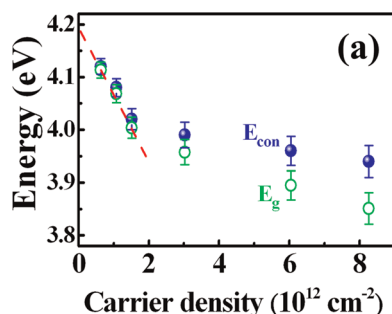

Fig. 4 Band-gap analysis. **a** E_{con} and E_g of the WS$_2$ MQDs with different carrier densities. **b** Schematic diagram showing the doping effect in the band structures of WS$_2$ MQDs.

where n, g_s, g_v, and q are charge density, valley degeneracy, spin degeneracy, and the hole charge, respectively. Considering the strong valley-spin locking in TMDs ($g_s g_v = 2$), E_g can be obtained from E_{con} by the following equation:

$$E_g = E_{con} - \frac{\hbar^2 k_F^2}{2m_e} - \frac{\hbar^2 k_F^2}{2m_h} = E_{con} - \frac{p\pi\hbar^2}{\mu q}, \tag{1}$$

where $\hbar$ is the reduced Planck constant, m_e and m_h are the effective electron and hole masses near K/K' point, respectively, and μ is the exciton reduced mass: $1/\mu = 1/m_e + 1/m_h$. The open circles in Fig. 4a show E_g versus p according to Eq. (1). The obtained E_g reveals nonlinear renormalization behavior as a function of p, where it drops pronouncedly as p is increased from $0.6(\pm 0.2) \times 10^{12}$ to $1.5(\pm 0.2) \times 10^{12}$ cm^{-2} and decreases moderately after $p = 1.5(\pm 0.2) \times 10^{12}$ cm^{-2}. A similar trend was reported for calculation of the band-gap in MoS$_2$ monolayers by a plasmon-pole theory.[28] The nonlinear band-gap evolution is attributed to large carrier-occupation energy and the carrier screening in two-dimensional semiconductors.[28] In Fig. 4a, E_g is largest at the lowest density (intrinsic doping) and the band-gap is strongly renormalized as p is increased. To determine the band-gap at the lowest density ($E_g(0)$) we extrapolated a line to E_g at the three lowest carrier densities (the dashed line in Fig. 4a). $E_g(0)$ was obtained from the intersection of the extrapolated line and the y-axis, and found to be ~4.19 eV. Accordingly, the band-gap renormalization $-\Delta E_g (=E_g(p) - E_g(0))$ versus p can be determined, as shown in Fig. 5. The $-\Delta E_g$ was found to decreases monotonously as p is increased. In a two-dimensional system, ΔE_g is expected to follow the remarkable power law[29,30]

$$-\Delta E_g \propto p^{\frac{1}{3}}, \tag{2}$$

The solid line in Fig. 5 displays the fitted line according to Eq. (2), which agrees with the measured $-\Delta E_g$. The shift of band-gap renormalization in WS$_2$ MQDs is ~250 ± 15 meV as p is increased from $0.6(\pm 0.2) \times 10^{12}$ to $8.3(\pm 0.2) \times 10^{12}$ cm^{-2}, which is larger than that (150 meV) for similar density changes in MoS$_2$ monolayers.[6] The large energy renormalization in WS$_2$ MQDs may be due to the reduced screening effect, which is more pronounced in TMD MQDs than in TMD monolayers. It is noted that, the simple power law (Eq. (2)) can well fit the shift of band-gap renormalization; however, more advanced calculation regarding band-gap renormalization in TMDs has been reported very recently, which may possibly be used to fit our data even better.[31,32]

Carrier-induced exciton binding energies

The exciton binding energy (E_b) in WS$_2$ MQDs can be calculated according to $E_b = E_g - E_{exc}$. Figure 6 shows E_b of the A-exciton in WS$_2$ MQDs versus p. The E_b decreases monotonically as p is increased. The WS$_2$ MQDs with the lowest p ($0.6(\pm 0.2) \times 10^{12}$ cm^{-2}) produces the largest E_b (~990 ± 30 meV), which is larger than the previous measured E_b in WS$_2$ and other TMD monolayers.[2,5] The huge exciton binding energy in our MQDs is ascribed to the extra quantum confinement in the lateral

dimension, which will be analyzed in the next paragraph. The band-gap renormalization and reduction of exciton binding energies in TMDs were mostly observed at cryogenic temperatures (50–80 K).[2,6] To our knowledge, this is the first demonstration of room-temperature many-body effects in semiconductors. More importantly, the band-gap and exciton binding energy can be tuned by varying p, which makes the WS$_2$ MQDs promising materials for developing exciton-based optoelectronic devices.[5]

Similar to $E_g(0)$, the E_b at the low density (E_{b0}) can be obtained by extrapolating a line to E_b at the four lowest carrier densities, as shown by the dashed line in Fig. 6. The E_{b0} was found to be as high as ~1.01 ± 0.03 eV, and this value is larger than the E_{b0} in the previous study of MoS$_2$ monolayers.[2] In MQDs, we estimate E_b using the following formula

$$E_b = E_0 + \frac{\hbar^2 \rho_0^2}{2(m_e + m_h)R^2} + \frac{\hbar^2 \rho_0^2}{2m_e R^2} + \frac{\hbar^2 \rho_0^2}{2m_h R^2}, \tag{3}$$

where E_0 is the exciton binding energy without in-plane confinement (i.e., the binding energy for a monolayer), R is the MQD radius (~2.5 nm), $m_e + m_h$ is the exciton effective mass, and ρ_0 ~2.405 is the first root of the zero-order Bessel function. The second term in the right side of Eq. (3) denotes the confinement effect for excitons. The third and fourth terms in the right side of Eq. (3) denote the confinement effect for the band-to-band transition. The lateral confinement effects due to both excitons and band-to-band transitions can be calculated and the result is about 0.2 eV. According to Eq. (3), we can deduce the exciton binding energy of WS$_2$ monolayers (E_0) by subtracting the energy of the confinement effects from the measured exciton binding energy in our MQDs (E_b). The obtained exciton binding energies of the WS$_2$ monolayers are about 0.99–0.84 eV as the carrier concentration varied from $0.6(\pm 0.2) \times 10^{12}$ to $8.3(\pm 0.2) \times 10^{12}$ cm^{-2}. These values are close to some previous experimental results (0.7–0.83 eV)[33–35] and theoretical calculations (0.5–1.05 eV)[36,37]; however, other experiments revealed the exciton binding energies of WS$_2$ monolayers at around 0.32–0.38 eV.[6,27] Obviously, there are discrepancies in the reports of the exciton binding energy in WS$_2$ monolayers. We suggest that the binding energy in TMDs can be affected by many factors such as carrier doping, substrate, strain, and other environmental effects.[34,38–40] This explains the diversity of the reported exciton binding energy in WS$_2$ monolayers.

DISCUSSION

The reduction of E_b with increasing free carriers in semiconductors has been interpreted by the carrier screening of the Coulomb interaction and phase-space filling.[8,24,41] However, by solving the gap equation with the screened Coulomb interaction, a recent report indicated that carrier screening is the dominant mechanism in TMD monolayers.[28] Thus, we only consider the screening effect for investigating the dependence of E_b on p. In general, the screening of Coulomb interactions reduces the influence of the dielectric environment and leads to a decrease of E_b. By increasing
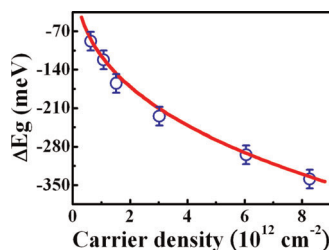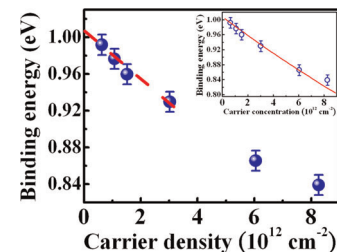

Fig. 5 Band-gap renormalization analysis. Band-gap renormalization of the WS$_2$ MQDs with different carrier densities. The solid line displays the fitted result using Eq. (2).

Fig. 6 Binding energy analysis. Exciton binding energies of A-excitons of the WS$_2$ MQDs with different carrier densities. The solid line in the inset shows the fitted result using Eq. (4).

carrier density, the Coulomb screening is increased and E_b will be further reduced. At a certain carrier density (Mott density), the excitons are completely ionized and the Mott transition occurs. By an equation analogous to the Debye screening, the resultant E_b due to the screening effect can be roughly estimated[42]

$$E_b = E_{bo} * e^{-\frac{p}{p_c}}, \tag{4}$$

where p_c is the Mott density. Using Eq. (4), E_b as a function of p was calculated, as shown in the solid line of the inset in Fig. 6. The fitted E_b agrees well with the experimental result, indicating that the reduction of E_b can be primarily interpreted by carrier screening. It is noted that the measured E_b is larger than the fitted one at the high carrier density ($p = 8.3 \times 10^{12}$ cm^{-2}), and this could be explained by contamination of the exciton peak with the DX states, which may enhance the red-shift of E_{exc} and increase E_b accordingly. In the fitting, The following parameters for WS$_2$ MQDs were used for fitting: $E_{b0} = 1.01 \pm 0.03$ eV and $p_c = 3.95 \times 10^{13}$ cm^{-2}. Here, p_c represents the critical carrier density for the Mott transition from excitons to electron–hole plasma, thus the p_c can be related to the exciton Bohr radius a_B according to the equation: $p_c = 2/\pi a_B$.[2,8,41] From the above equation, a_B was obtained to be ~1.27 nm, which is close to the one (~1 nm) reported from the WS$_2$ monolayer.[7] Therefore, we deduce that the complete ionization of the excitons in WS$_2$ MQDs occurs at p_c ~3.95 × 10^{13} cm^{-2} or a_B ~1.27 nm.

This work observed the band-gap renormalization and reduction of exciton binding energies in DETA-doped WS$_2$ MQDs. However, other interesting phenomena in many-body effects, such as the Mott transition or formation of charged excitons have not been observed yet, which is our intended future work. In addition, functionalization of WS$_2$ MQDs by different doping agents such as thiols or amino acid may offer the possibility to modify the physical properties of WS$_2$ MQDs, and thus, provide a vehicle for the investigation of fundamental science in two-dimensional materials.

In summary, many-body effects in doped WS$_2$ MQDs were studied at room temperature using PLE and the absorption spectra. By measuring the onset of continuum absorption and considering the Pauli blocking effect in a parabolic dispersion, E_g of WS$_2$ MQDs for p from 0.6($\pm$0.2) × 10^{12} to 8.3($\pm$0.2) × 10^{12} cm^{-2} was obtained. The resulting renormalization in E_g was found to be as large as ~250 ± 15 meV, which is larger than that in MoS$_2$ monolayers for similar density changes. The binding energy E_b of A-exciton in WS$_2$ MQDs was analyzed as a function of p. An exciton binding energy of ~990 ± 30 meV was obtained for the WS$_2$ MQDs with the lowest carrier density, which is larger than that observed in WS$_2$ and other TMD monolayers. The huge exciton binding energy in WS$_2$ MQDs is a consequence of the extra quantum confinement in the lateral dimension. Compared to TMD monolayers, the large band-gap renormalization and exciton binding energies in WS$_2$ MQDs could be due to the efficient reduced screening of the Coulomb interaction in the quantum-disk structure. In addition, the critical carrier density for Mott transition from excitons to free carriers in WS$_2$ MQDs was estimated to be 3.95×10^{13} cm^{-2}. Our result represents the first ever reported demonstration of the effects of band-gap renormalization and reduction of exciton binding energies in semiconductors at room temperature. This work is expected to be very useful for developing exciton-based optoelectronic and photonic devices derived from two-dimensional materials.

METHODS

Synthesis of WS$_2$ MQDs. The WS$_2$ nanoflakes, purchased from *Graphene Supermarket* (USA), were suspended in ethanol (~2.57 mg/mL) with DETA, purchased from *Sigma-Aldrich*, in a quartz bottle and thoroughly mixed using a vortex shaker. DETA concentration was varied from 16 to 800 mM to change the carrier density in WS$_2$.[43] The WS$_2$ suspension was exposed to laser pulses with duration of 10 ns, a wavelength of 415 nm, and a repetition rate of 10 Hz on a rotational stage with an angular velocity of 80 rpm. Pulsed laser ablation (PLA) of the WS$_2$ suspension was carried out under the fluence of 2.6 J/cm^2 for 30 min. After PLA, the suspension product was centrifuged at 6000 rpm, and then, filtered by a syringe filter (Millipore, 0.22 μm pore size). After centrifugation the synthesized WS$_2$ MQDs were diluted by dialysis using a 0.1–0.5 kDa membrane for 2 days.

Characterization of WS$_2$ MQDs. The charge transport properties of the DETA-doped WS$_2$ MQDs were characterized by a field-effect transistor (FET) device. The device was fabricated using heavily doped p-type Si substrates with a 100 nm thick SiO$_2$ capping layer in a back-gated configuration. The channel length and width of the device were around 40 and 160 μm, respectively. Source and drain contacts of Ti/Al were deposited by an electron beam evaporator. The image of the device is shown in the inset of Supplementary Fig. S7b. A 1 μl of WS$_2$ MQD solution was drop casted onto the electrode pattern and dried at 60 °C for 30 min. The electrical measurements of the back-gated FET were performed on a microprobe station by using a semiconductor parameter analyzer (HP 4145B). Supplementary Fig. S7a shows the drain current I_d versus the gate voltage for WS$_2$ MQDs with various DETA concentrations. The carrier density p was calculated from the shift of the threshold voltage (V_{th}) according to the equation:[43,44] $p = C_g \Delta V_{th}/q$, where C_g, ΔV_{th}, and q are the capacitance of SiO$_2$ per unit area, the difference of V_{th}, and the elementary charge, respectively. By analyzing the ΔV_{th} from the I_d-V_g curves, p was estimated and displayed in Supplementary Fig. S7b. The carrier density in WS$_2$ MQDs was found to change from 0.6($\pm$0.2) × 10^{12} to 8.3($\pm$0.2) × 10^{12} cm^{-2} due to doping with different DETA concentrations. It is noted that the electrical measurement was performed on the MQD ensemble, not on the individual MQD. Under the electrical characterization, some carriers would be trapped or captured by the defect/edge states generated from laser ablation, while other free carriers would become conduction carriers and produce the electric currents in FET. Thus, the carrier concentrations measured from FET can be applicable to MQDs. Similar methods have been used to estimate the carrier concentration in reduced graphene oxide.[45]

A high resolution transmission electron microscope (JEOL JEM-2100F) with operating voltage of 200 kV was used to analyze the size of WS$_2$ MQDs. An AFM system (PSIA XE-100) in a tapping mode was used to determine the height and surface roughness of WS$_2$ MQDs. The PL and PLE spectra of WS$_2$ MQDs were measured using a Horiba Jobin Yvon FluoroMax-4 spectrofluorometer. The optical absorption measurements were performed using a JASCO V-750 spectrophotometer. All measurements were carried out at ambient temperature.

REFERENCES

1. Wang, H. et al. Radiative lifetimes of excitons and trions in monolayers of the metal dichalcogenide MoS$_2$. *Phys. Rev. B* **93**, 045407 (2016).
2. Yao, K. et al. Optically discriminating carrier-induced quasiparticle band gap and exciton energy renormalization in monolayer MoS$_2$. *Phys. Rev. Lett.* **119**, 087401 (2017).
3. Mak, K. F. et al. Tightly bound trions in monolayer MoS$_2$. *Nat. Mater.* **12**, 207–211 (2013).
4. Ross, J. S. et al. Electrical control of neutral and charged excitons in a monolayer semiconductor. *Nat. Commun.* **4**, 1474 (2013).
5. Mak, K. F. & Shan, J. Photonics and optoelectronics of 2D semiconductor transition metal dichalcogenides. *Nat. Photonics* **10**, 216–226 (2016).
6. Chernikov, A. et al. Electrical tuning of exciton binding energies in monolayer WS$_2$. *Phys. Rev. Lett.* **115**, 126802 (2015).
7. Chernikov, A., Ruppert, C., Hill, H. M., Rigosi, A. F. & Heinz, T. F. Population inversion and giant bandgap renormalization in atomically thin WS$_2$ layers. *Nat. Photonics* **9**, 466–470 (2015).
8. Liu, B. et al. Engineering bandgaps of monolayer MoS$_2$ and WS$_2$ on fluoropolymer substrates by electrostatically tuned many-body effects. *Adv. Mater.* **28**, 6457–6464 (2016).

9. Gao, S., Liang, Y., Spataru, C. D. & Yang, L. Dynamical excitonic effects in doped two-dimensional semiconductors. *Nano Lett.* **16**, 5568–5573 (2016).

10. Steinhoff, A. et al. Exciton fission in monolayer transition metal dichalcogenide semiconductors. *Nat. Commun.* **8**, 1166 (2017).

11. Lin, L. et al. Fabrication of luminescent monolayered tungsten dichalcogenides quantum dots with giant spin-valley coupling. *ACS Nano* **7**, 8214–8223 (2013).

12. Wilcoxon, J. P. & Samara, G. A. Strong quantum-size effects in a layered semiconductor: MoS_2 nanoclusters. *Phys. Rev. B* **51**, 7299–7302 (1995).

13. Bhuyan, S., Jindal, V., Jana, D. & Ghosh, S. Signatures of self-trappping of trions in monolayer MoS_2. *J. Phys. D* **51**, 435102 (2018).

14. You, Y. et al. Observation of biexcitons in monolayer WSe_2. *Nat. Phys.* **11**, 477–481 (2015).

15. Wang, H., Zhang, C. & Rana, F. Ultrafast dynamics of defect-assisted electron-hole recombination in monolayer MoS_2. *Nano Lett.* **15**, 339–345 (2015).

16. Aleithan, S. H. et al. Broadband femtosecond transient absorption spectroscopy for a CVD MoS_2 monolayer. *Phys. Rev. B* **94**, 035445 (2016).

17. Jiang, T., Chen, R., Zheng, X., Xu, Z. & Tang, Y. Photo-induced excitonic structure renormalization and broadband absorption in monolayer tungsten disulphide. *Opt. Exp.* **26**, 859 (2018).

18. Delalande, C. et al. Many-body effects in a modulation-doped semiconductor quantum well. *Phys. Rev. Lett.* **59**, 2690–2692 (1987).

19. Tuan, D. V. et al. Probing many-body interactions in monolayer transition-metal dichalcogenides. *Phys. Rev. B* **99**, 085301 (2019).

20. Dery, H. Theory of intervalley Coulomb interactions in monolayer transition-metal dichalcogenides. *Phys. Rev. B* **94**, 075421 (2016).

21. Groenewald, R. E., Rösner, M., Schönhoff, G., Haas, S. & Wehling, T. O. Valley plasmonics in transition metal dichalcogenides. *Phys. Rev. B* **93**, 205145 (2016).

22. Sie, E. J., Frenzel, A. J., Lee, Y.-H., Kong, J. & Gedik, N. Intervalley biexcitons and many-body effects in monolayer MoS_2. *Phys. Rev. B* **92**, 125417 (2015).

23. Park, Y. et al. Interplay between many body effects and Coulomb screening in the optical bandgap of atomically thin MoS_2. *Nanoscale* **9**, 10647–10652 (2017).

24. Meckbach, L., Stroucken, T. & Koch, S. W. Giant excitation induced bandgap renormalization in TMDC monolayers. *Appl. Phys. Lett.* **112**, 061104 (2018).

25. Steinhoff, A., Rösner, M., Jahnke, F., Wehling, T. O. & Gies, C. Influence of excited carriers on the optical and electronic properties of MoS_2. *Nano Lett.* **14**, 73743–3748 (2014).

26. Borys, N. J. et al. Anomalous above-gap photoexcitations and optical signatures of localized charge puddles in monolayer molybdenum disulfide. *ACS Nano* **11**, 2115–2123 (2017).

27. Chernikov, A. et al. Exciton binding energy and nonhydrogenic Rydberg series in monolayer WS_2. *Phys. Rev. Lett.* **113**, 076802 (2014).

28. Liang, Y. & Yang, L. Carrier plasmon induced nonlinear band gap renormalization in two-dimensional semiconductors. *Phys. Rev. Lett.* **114**, 063001 (2015).

29. Kleinman, D. A. & Miller, R. C. Band-gap renormalization in semiconductor quantum wells containing carriers. *Phys. Rev. B* **32**, 2266–2272 (1985).

30. Rossbach, G. et al. High-temperature Mott transition in wide-band-gap semiconductor quantum wells. *Phys. Rev. B* **90**, 201308 (2014).

31. Tuan, D. V., Scharf, B., Žutić, I. & Dery, H. Marrying excitons and plasmons in monolayer transition-metal dichalcogenides. *Phys. Rev. X* **7**, 041040 (2017).

32. Scharf, B., Tuan, D. V., Žutić, I. & Dery, H. Dynamical screening in monolayer transition-metal dichalcogenides and its manifestations in the exciton spectrum. *J. Phys.* **31**, 203001 (2019).

33. Ye, Z. et al. Probing excitonic dark states in single-layer tungsten disulphide. *Nature* **513**, 214–218 (2014).

34. Zhu, B., Chen, X. & Cui, X. Exciton binding energy of monolayer WS_2. *Sci. Rep.* **5**, 9218 (2015).

35. Hanbicki, A. T., Currie, M., Kioseoglou, G., Friedman, A. L. & Jonker, B. T. Measurement of high exciton binding energy in monolayer transition-metal dichalcogenides WS_2 and WSe_2. *Solid State Commun.* **203**, 16–20 (2015).

36. Berkelbach, T. C., Hybertsen, M. S. & Reichman, D. R. Theory of neutral and charged excitons in monolayer transition metal dichalcogenides. *Phys. Rev. B* **88**, 045318 (2013).

37. Ramasubramaniam, A. Large excitonic effects in monolayers of molybdenum and tungsten dichalcogenides. *Phys. Rev. B* **86**, 115409 (2012).

38. Tuan, D. V., Yang, M. & Dery, H. Coulomb interaction in monolayer transition-metal dichalcogenides. *Phys. Rev. B* **98**, 125308 (2018).

39. Keliang, H. et al. Tightly bound excitons in monolayer WSe_2. *Phys. Rev. Lett.* **113**, 026803 (2014).

40. Stier, A. V. et al. Magnetooptics of exciton Rydberg states in a monolayer semiconductor. *Phys. Rev. Lett.* **120**, 057405 (2018).

41. Huang, D., Chyi, J. & Morkoç, H. Carrier effects on the excitonic absorption in GaAs quantum-well structures: phase-space filling. *Phys. Rev. B* **42**, 5147–5153 (1990).

42. Liu, W. et al. Carrier-density-dependent recombination dynamics of excitons and electron-hole plasma in *m*-plane InGaN/GaN quantum wells. *Phys. Rev. B* **94**, 195411 (2016).

43. Caigas, S. P. et al. P-type doping of WS_2 quantum dots via pulsed laser ablation. *ACS Photon.* **5**, 4828–4837 (2018).

44. Tarasov, A. et al. Controlled doping of large-area trilayer MoS_2 with molecular reductants and oxidants. *Adv. Mater.* **27**, 1175 (2015).

45. Kobayashi, T., Kimura, N., Chi, J., Hirata, S. & Hobara, D. Channel-length-dependent field-effect mobility and carrier concentration of reduced graphene oxide thin-film transistors. *Small* **6**, 1210 (2010).

AUTHOR CONTRIBUTIONS

J. L. Shen conceived the idea. T. N. Lin and S.R.M. Santiago designed and performed the experiments. S. P. Caigas synthesized the materials. C. T. Yuan and T. Y. Lin helped with the optical measurements. T. N. Lin, S. R. M. Santiago, J. L. Shen and Y. F. Chen analyzed the data and were involved in writing the paper. T. N. Lin and S. R. M. Santiago contributed equally to this work and are assigned as co-first authors.

COMPETING INTERESTS

The authors declare no competing interests.

ADDITIONAL INFORMATION

Supplementary information is available for this paper at https://doi.org/10.1038/s41699-019-0129-z.

Correspondence and requests for materials should be addressed to J.L.S.

Reprints and permission information is available at http://www.nature.com/reprints

Publisher's note Springer Nature remains neutral with regard to jurisdictional claims in published maps and institutional affiliations.